PROCEEDINGS, Thirty-Seventh Workshop on Geothermal Reservoir Engineering
Stanford University, Stanford, California, January 30 - February 1, 2012
SGP-TR-194

APPROACH FOR DETERMINATION OF THE FAILURE PROBABILITY OF FRACTURES AT THE SOULTZ-SOUS-FORÊTS EGS PROJECT

Carola Meller, Thomas Kohl, Emmanuel Gaucher, Albert Genter

Karlsruhe Institute of Technology (KIT)
Kaiserstraße 12
Karlsruhe, Baden-Württemberg, 76131, Germany
e-mail: carola.meller@kit.edu

ABSTRACT

Borehole stimulation in Enhanced Geothermal Systems (EGS) in order to improve the reservoir permeability is commonly accompanied with induced seismicity. These microearthquakes are caused by shearing of (pre-existing) fracture planes. In the present study an approach for estimation of the shearing probability of the fractures based on statistical analyses of fracture distribution, orientation and clusters, is proposed.

Based on geophysical logs of five wells in Soultz-sous-Forêts, France, and with the help of statistical tools, the Mohr criterion, geological and mineralogical properties of the host rock and the fracture fillings, correlations between the geothermal wells are analyzed. This is achieved with the MATLAB-code *Fracdens* developed by us, which enables us to statistically analyze the datasets with depth. In a first step this is done with a focus on the orientational features of the fractures. By scanning the wells in depth intervals of 150 m, we can observe the evolution of fracture clusters with different orientation. The clusters occur at certain depths and are mainly subvertical fracture sets. The application of the Mohr Coulomb failure criterion enables us to estimate the distribution of the critical pressure of the fractures with depth. We show that the application of the Terzaghi correction for borehole orientation bias significantly influences the evaluation of the dataset, especially on the estimation of the critical pressure. Without applying the correction we can see much more critically stressed fractures than after correcting for orientation bias.

In a further step we want to virtually apply a pore pressure perturbation on the reservoir to observe the evolution of the critical pressure on the fractures and thus get an idea about the mechanical response of the fractures to the pressure perturbation. A special focus is on the clay fillings of the fractures as they can reduce the frictional strength of the reservoir rock and thus determine its mechanical behavior.

INTRODUCTION

Motivation

In recent times the search for alternative sources of energy has been fostered by the scarcity of fossil fuels. With its ability to permanently provide electricity or heat with little emission of CO_2, geothermal energy will have an important share in the energy mix of the future. Within Europe, scientists identified many locations with conditions suitable for EGS projects. In order to provide sufficiently high reservoir permeability, EGS require borehole stimulations prior to installation of power plants (Gérard et al, 2006). People living near EGS projects are sometimes frightened by induced earthquakes occurring during stimulation or injection. As the occurring (micro)seismicity is a factor that presently cannot be predicted nor can be controlled, it is appreciable to find a way to estimate the probability of fractures to shear when injecting water with a distinct pressure into a geothermal reservoir. This knowledge would enable us to predict the mechanical behavior of a reservoir in response to a change in pore pressure conditions.

Soultz-sous-Forêts EGS site

The Enhanced Geothermal System at Soultz-sous-Forêts in Alsace, France was set up as a research site and has been investigated for decades. It provides us an outstanding database of borehole data and scientific work of scientists from all over the world.

The Soultz site is located in a region with an increased geothermal gradient in the western part of the Upper Rhine Valley where a temperature of 100°C is reached at a depth of 1km. The valley is a Cenozoic rift structure, which is part of the West European Rift System (Figure 1, Dezayes et al., 2010). The reservoir of the EGS system is in a depth of 5000m and the geothermal power plant produces water at a temperature of ~168°C. Since 2008 it provides a capacity of 1.5 MW_e (Genter et al, 2010).

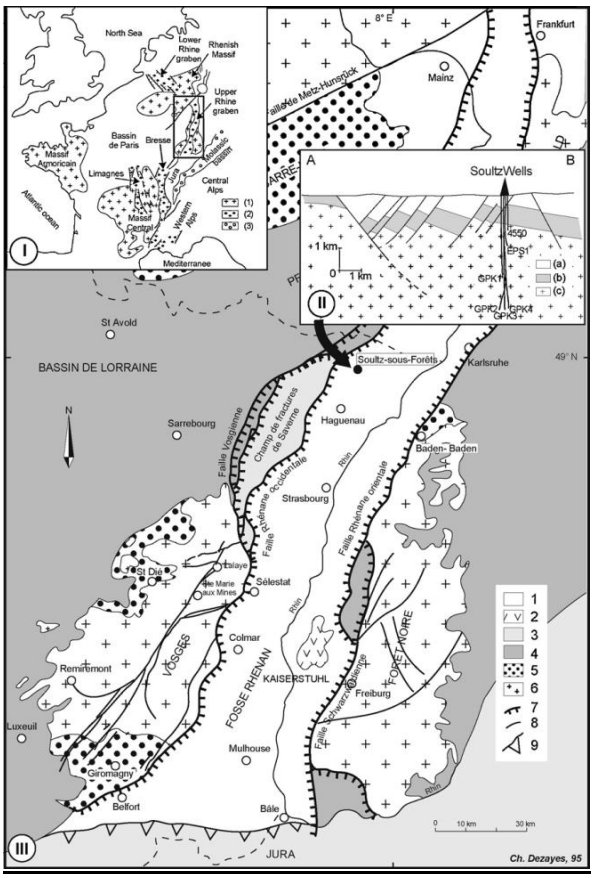

Figure 1: Structural map of the Upper Rhine Valley. The black arrow (II) shows the location of the Soultz-sous-Forêts site. (a) Cenozoic; (b) Mesozoic; (c) Hercynian basement; (1) Cenozoic sediments; (2) Cenozoic volcanics; (3) Jurassic; (4) Triassic; (5) Permo-Carbonifeous basins, (6) Hercynian basement; (7) boundary faults; (8) other faults; (9) overthrusts. (after Dezayes, 2000)

Geological description of the reservoir

The geothermal reservoir of the EGS mainly consists of three different kinds of fractured granites, a porphyritic feldspar-rich monzogranite (standard granite) rich in cm-sized feldspar crysts, biotite/amphibole-rich granite xenoliths within the standard granite, and a fine-grained two-mica granite at depths below 4500 m (Hooijkaas et al., 2006). The naturally occurring fractures are mainly filled. The fillings contain various minerals, whereas the most abundant are calcite, quartz, illite, and other clay minerals (e.g. Genter et al, 1997). The thickness of the fractures varies between 0.5 mm and 250 mm (Genter & Traineau, 1996) and their density and orientation vary with depth (Dezayes et al, 2000). In some zones the rock is hydrothermally altered in different scales. Hydrothermal alteration has taken place in all three kinds of granite where it often goes ahead with a transformation of primary minerals (mainly biotite and plagioclase) into secondary minerals (clay minerals), but without changing the primary rock texture (Hooijkaas et al., 2006).

DATABASE

Logs

The various logs, which are the basis of this study, were measured in the years between 1987 and 2009. The quality, the amount of available data and the covered depths vary between the five wells and also with the kind of log. Image logs are mostly universal borehole imager logs (UBI). These UBI logs are the basis for the fault orientation analysis, as well as lithologs and Gamma ray (GR) are available for all wells, whereas continuous logging exists for EPS1 only. The wells GPK1, GPK2, GPK3 and GPK4 are were fully logged from the top of the granite to depths of ~3600m, first logged to ~3900m then deepened to 5000m, and ~5100m respectively.

State of stress

The state of stress at the Soultz-sous-Forêts site was determined by several studies on the basis of mainly borehole breakouts and hydraulic tests (e.g. Rummel & Klee, 1995; Cornet et al., 2007; Valley, 2007). In the present study we use the most recent stress state model from Cornet et al., 2007 and Valley, 2007. The latter one is an extension of Cornet's model to greater depths. The evolution of the principal effective stress components with depth is shown in Figure 2) and is described by the equations (1) to (4).

$$\sigma_v[MPa] = -1.30 + 25.5 \cdot z[km] \pm(0.98 \cdot z[km] + 0.6) \quad (1)$$

$$\sigma_h[MPa] = -1.78 + 14.09 \cdot z[km] \pm(0.45 \cdot z[km] + 1.82) \quad (2)$$

$$\sigma_H[MPa] = 0.75 \cdot \sigma_v \; to \; 1.15 \cdot \sigma_v \quad (3)$$

(maximum uncertainty, variation depends on depth)

$$P_p[MPa] = 0.9 + 9.8 \cdot z[km] \quad (4)$$

whereas σ_v, σ_H and σ_h are the vertical, the maximum horizontal and the minimum horizontal principal stress and P_p is the pore pressure, z is the depth in km. We must keep in mind, however, that there is a large uncertainty about the absolute values of the stress components, especially for σ_H.

The upper part of the Soultz reservoir is dominated by a normal stress regime ($\sigma_h > \sigma_H$), whereas in the deeper part of the reservoir (i.e. below a depth of 3.5km) a strike-slip regime dominates ($\sigma_h < \sigma_H$).

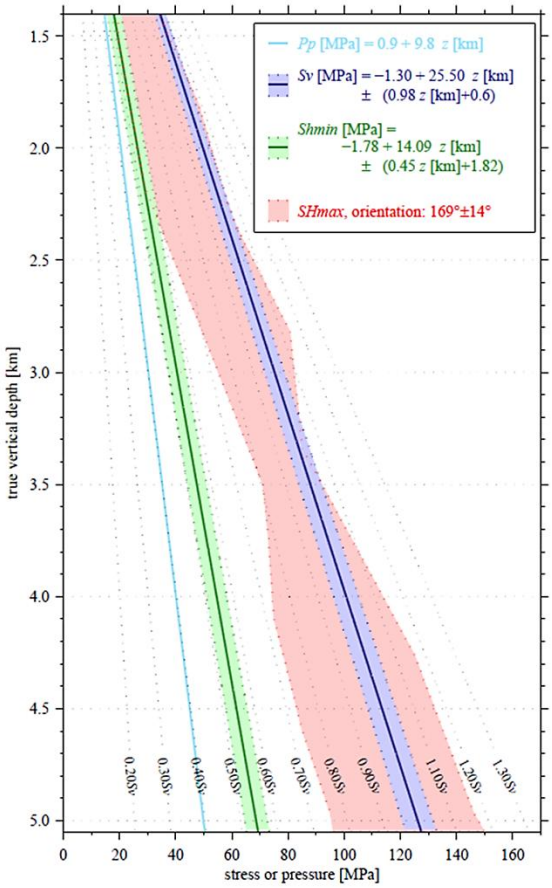

Figure 2: The state of stress in the Soultz-sous-Forêts geothermal reservoir (after Valley, 2007).

BACKGROUND AND TOOLS

The logging data provide us detailed information about the reservoir lithology and fracture density and distribution with depth. Gamma ray and caliper logs give us highly resolved evidence of the element distribution and the prevailing mineralogy at a given depth (in cm-scale). The idea for the present study is to combine these data with frictional properties of the reservoir rocks and fracture fillings. For this purpose, we wrote the MATLAB code *Fracdens* to process the raw logging data. The analysis of data with this code is described in the following chapter.

Database

For the analysis we use the logging data from the boreholes EPS1 and GPK1-4, which include image logs, gamma ray, caliper, lithologs, and fracture geometry (Dezayes et al., 2000). For EPS1 a continuous coring is available. For the examples shown below only UBI data from the well GPK3 is used.

Fracdens

The *Fracdens* code is a tool to analyze the borehole data from different points of view. For this purpose we can filter the data with respect to the well, the logging tool and the required depth or depth interval to be scanned. We have to input the logs as raw data, a stress field and the friction parameters of the reservoir. The program then starts its analysis automatically. The single steps are shown below.

Stereografic distribution

One of the common tools for directional statistics is the stereographic projection. This visualization method allows us to qualitatively find the main orientations of fractures and helps to identify clusters (Figure 3).

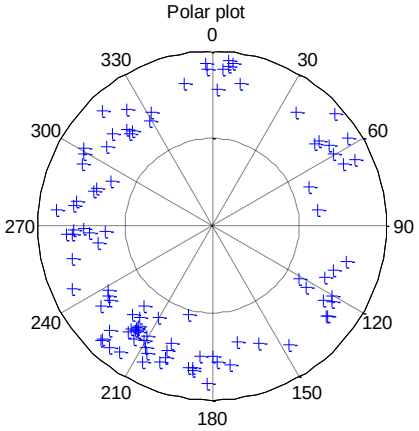

Figure 3: Stereografic plot (lower hemisphere) of the fracture normals for a depth interval of 4500 to 4650m in GPK3. The numbers around the stereogram show the azimuthal deviation from north. The radial scale reaches from a dip angle of 0° (horizontal fracture) in the center of the stereogram to 90° at the outer rim (vertical fracture).

However, it would be appreciable to quantitatively analyze the orientations. The azimuthal histogram (Figure 4) helps determining the main dip directions. It neglects, however the dip angle. Therefore, a new method is suggested to visualize fracture dips and directions and allows a semi-quantitative analysis of fracture density in certain dip directions and dip angles. The idea is to subdivide the stereographic plot into bin of equal area. This is done after a method developed by R.J. Fryer (1975). He iteratively determined the azimuths of meridians that mark the border of elements within bounding parallels in a way that they are very similar in shape and equal in area.

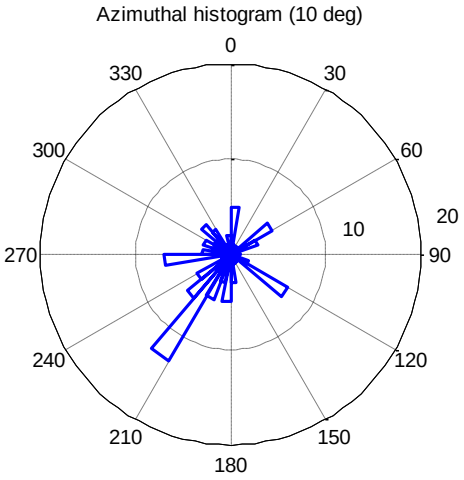

Figure 4: Azimuthal histogram (lower hemisphere) of the fracture normasl for a depth interval of 4500 to 4650m in GPK3. Radially depicted numbers are the dip from vertical in degrees.

Instead of plotting the number of fractures, the fracture density in the respective depth interval is given by the color of the bin (Figure 5). Thus, this plot makes it possible to qualitatively and semi-quantitatively find fracture family sets. If needed, the number and hence the size of the bins can be adjusted in certain values between 6 and 470. These numbers are fixed by Fryer's method of subdividing the sphere (more detailed information can be found in Fryer, 1975).

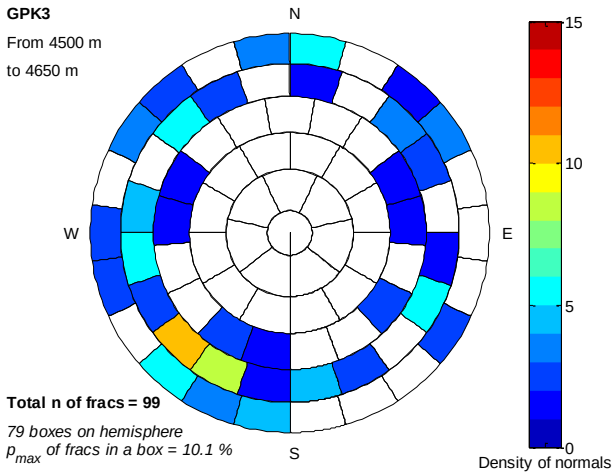

Figure 5: Fryer-plot (lower hemisphere) of fracture density in GPK3 (4500-4650m) in 79 bins of equal area. Dip angles refer to the fracture normals.

Terzaghi-Correction of fracture density

When sampling 3D fracture orientation data in 2D structures like boreholes, there is always the problem of linear sampling bias. When a borehole cuts a fracture set at an angle between borehole and normal on the set, the fracture density on this section is smaller than it would be at a smaller cutting angle (Figure 6). Terzaghi (1965) suggested a method, which corrects the fracture density according to the cutting angle with the borehole by introducing a geometrical weighting factor:

$$n_{fracs} = \frac{1}{\cos \alpha} \qquad (5)$$

The number of fractures in an interval n_{fracs} is corrected by the reciprocal cosine of the cutting angle between fracture normal and borehole α.

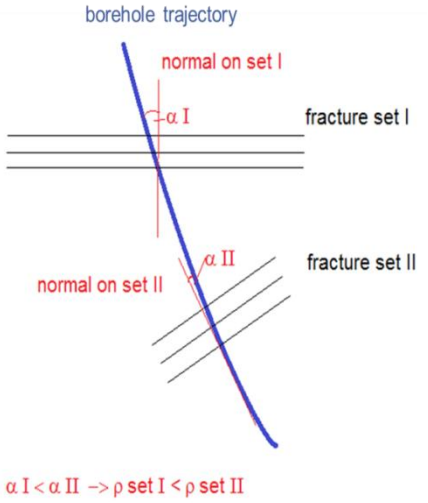

Figure 6: Linear sampling bias due to the cutting angle between fracture sets and the borehole.

The problem of this correction is an overestimation of fractures subparallel to the borehole (Yow, 1987), where $n_{fracs} \rightarrow \infty$. Therefore, a maximum allowed correction angle α_{max} is defined.

$$\alpha_{max} = \cos^{-1}\left(\frac{l_i}{l_s}\right) \qquad (6)$$

The lengths l_i and l_s are the length of the sampling interval and the maximum thickness of a geological unit. In this study, l_i is 150m and l_s is estimated to 1500m. Thus, the maximum correction angle is $\alpha_{max} \approx 5.7°$. Figure 7 shows the effect of this correction on the stereoplot. The density of steeply dipping fractures (outer annuli) has increased.

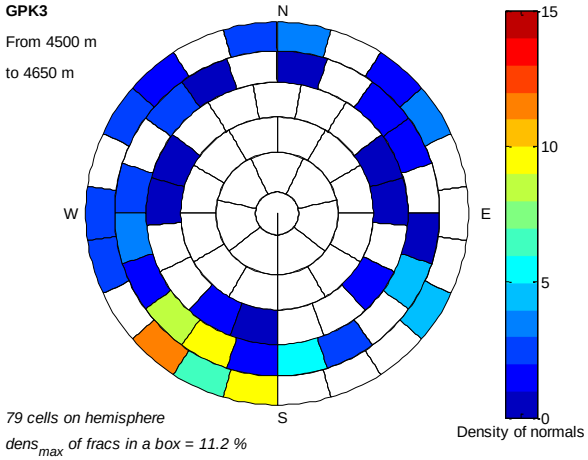

Figure 7: Fryer plot from Figure 5 after application of the Terzaghi correction.

Mohr-Coulomb friction analysis

If we want to analyze the fracture stability according to their orientation in the prevailing stress field, we have to analyze the fracture data Mohr-Coulomb analysis.

The Mohr-diagram is a practical and demonstrative tool for analyses of rock and fracture stability in a given stress field. It requires knowledge of the prevailing stress and pore pressure which is provided by the work of Valley, 2007. Furthermore, one has to know the fracture orientation relative to the principal stress axes. This can be calculated from the fracture orientation data derived from borehole image logs. The remaining parameters to be known is the frictional strength (friction coefficient $tan\ \theta$) and the cohesion c of the rock. For a first approach we assume $tan\ \theta$ to be in the limits of 0.6 and 1.0, the conservative bounds for planar interfaces in rock (Byerlee, 1978) and c be 4MPa (Cornet et al., 2007). The friction law

$$\tau = \sigma_n \tan\theta + c \qquad (4)$$

with τ the shear stress on the fracture plane and σ_n the normal stress on the plane, allows drawing the fractures into a Mohr circle diagram for a given depth (Figure 8).

A pore pressure change has no influence on the deviatoric stress (i.e. the radius of the circles), but it will only move the circles to the right (pore pressure decrease) or to the left (pore pressure increase). This is what happens during injection into or production from a geothermal well. The effect of a pore pressure increase by 10MPa is shown in Figure 9.

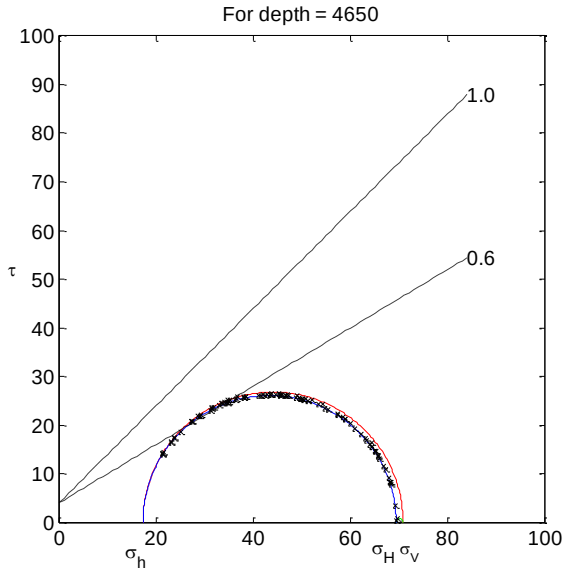

Figure 8: Mohr diagram for the fractures in a 150m interval of GPK3 in a depth interval of 4500m to 4650m and the state of stress at 4650m.

After injection of water with a pressure of 10MPa, all fractures that lie now between the two failure envelopes and have a friction coefficient of 0.6 have sheared, which means their critical pressure was reached. In this context the critical pressure is taken as the distance of the fractures from the failure envelope. This allows us to quantify the reaction of the fractures to pore pressure changes.

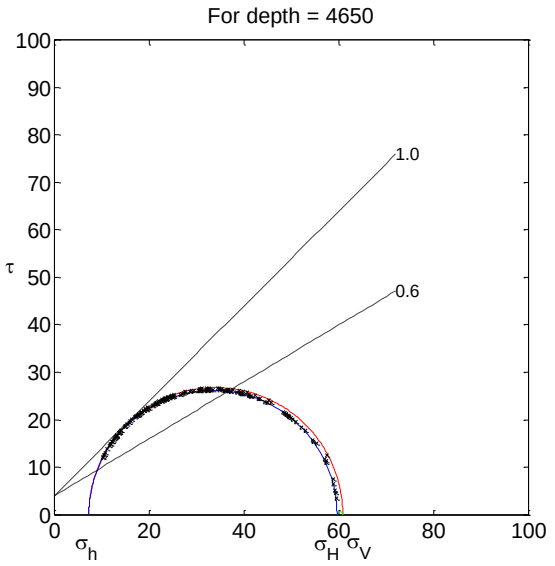

Figure 9: Mohr circle from Figure 8 after a 10MPa increase of pore pressure (e.g. during stimulation).

Determination of the Critical Pressure

The distance of a single fracture in the Mohr circle from the failure envelope gives us the pressure needed to shear this fracture, here referred to as the critical pressure P_c. A histogram of the distribution of P_c for the depth interval of 4500 to 4650m in GPK3 suggests a relationship between the numbers of fractures with a distinct critical pressure and the amount of P_c, which shows rapidly decreasing numbers of fractures with increasing P_c (Figure 10). The friction coefficient is assumed to be 0.6 here, although this value is too low for massive granite.

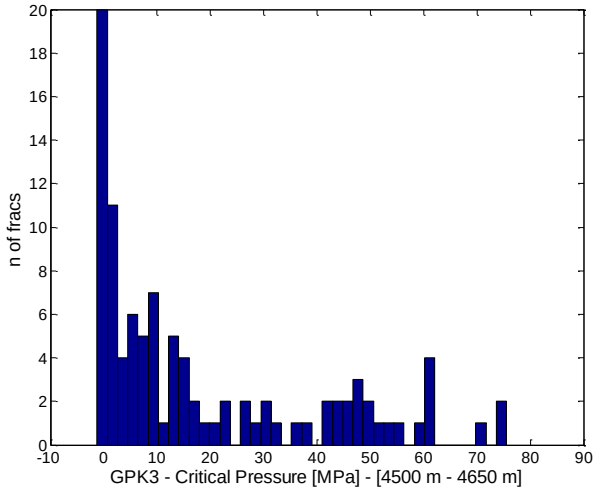

Figure 10: Distribution of the critical pressure in the depth interval of 4500 to 4560m of GPK3. The friction coefficient is 0.6. Low values of P_p are evidence of critically stressed fractures that can shear due to small changes of pressure conditions.

A negative value of P_c occurs when fractures have already sheared under equilibrium conditions.

The exponential distribution of the critical pressure with a lot of critically stressed fractures however, is only a result of sampling bias. After weighting the samples by the Terzaghi correction factor the distribution of P_c looks totally different (Figure 11). Here, we can see a lot more fractures with a high critical pressure, which means that they are far away from the failure envelope and thus will only shear when the injection pressure is much higher than 30 MPa. The P_c analysis provides a possibility to get an overview over the stress situation in the reservoir and which fractures can be expected to shear due to a certain change in pressure conditions. The next step is to combine the directional data with the calculation of P_c in order to find relationships between dipping angle, azimuth and the frictional behavior of fractures or fracture sets.

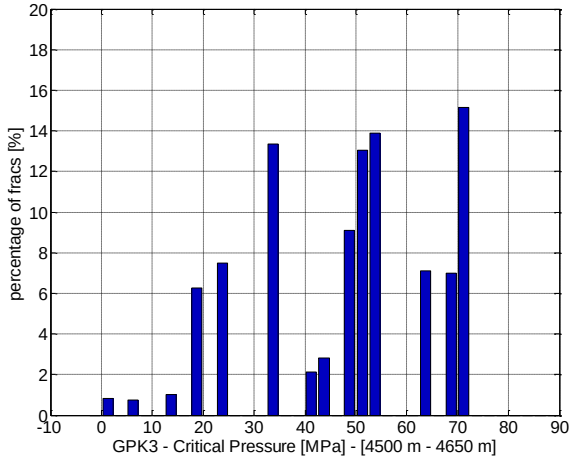

Figure 11: Distribution of the critical pressure between 4500m and 4650m as shown in Figure 10, but after Terzaghi correction of the fractures. The friction coefficient is 0.6.

In this way, the critical pressure distribution all along the borehole can be determined and combined in a single plot. This is shown in Figure 12. The reason for the increase of the value for P_c with depth is the increasing effective stress.

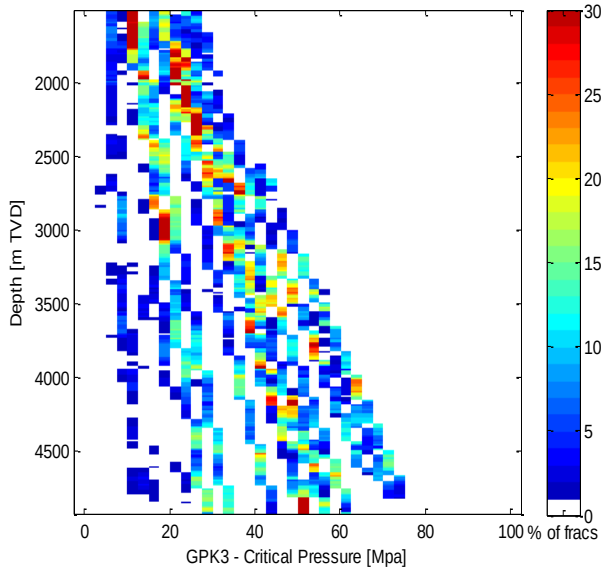

Figure 12: Distribution of the critical pressure along the GPK3 borehole. It shows the critical pressure (x-axis) and the respective density of fractures with the respective P_c with depth. The colors represent the percentage of fractures in one depth interval (each box represents 15m) with a distinct critical pressure.

The combination of critical pressure and orientation

After subdivision of the fracture set into bins of dip angle and azimuth intervals, the critical pressure can be calculated as a function of the fracture orientation. For this calculation, the mean orientation of the respective fractures in a bin is taken. The mean dip and strike of a bin is calculated by the mean values of the bin boundaries and the Terzaghi correction is applied.

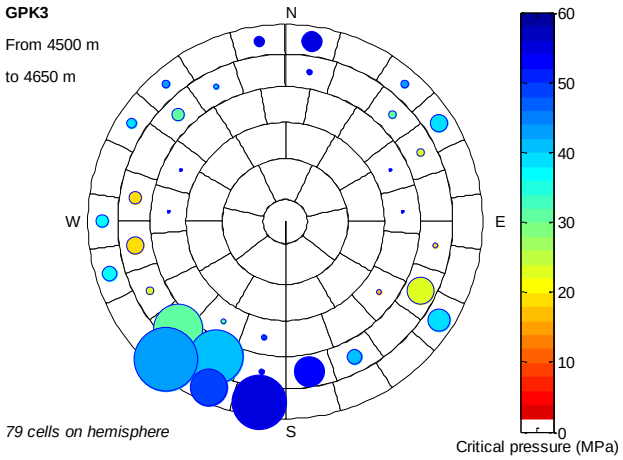

Figure 13: Modified Fryer stereo plot for the depth interval 4500m to 4650m in GPK3, which combines the information from Figure 7 and Figure 12. The circles are coloured according to the critical pressure of the bin and their size represents the fracture density.

PROCEDURE

For a detailed analysis of the Soultz data we have to meet several challenges. In the examples above we assumed the friction coefficient to be constant along the borehole. In reality, this coefficient varies strongly depending on the lithology and structure of the fractures. Massive granite, for example, has a much higher friction coefficient than clay minerals that are present in the fractures. We can however not postulate that the friction coefficient in a fracture is equal to that of the fracture filling mineral. Therefore, the fracture fillings have to be carefully identified and the mechanical behavior of the fractures with certain fillings has to be investigated in laboratory measurements.

Log analysis

For a detailed analysis of the fracture fillings the new tool called Techlog from Schlumberger will be used. It allows the identification of certain parameters according to characteristics of physical logging data. The aim is to allocate the mineralogy of fracture fillings to the different identified fracture zones.

Reference measurements

For Soultz, there is a lot of information about the reservoir available as logging data. As the Soultz granite is hidden by 1.5km of sediments, it is not possible to investigate the petrophysical properties in detail.Moreover, there is very little core material or samples. For laboratory measurements, we have to find reference sites with similar lithology and fracture structures. Additional data will be taken from measurements of artificial fractures in order to determine the dynamic behavior of fractures due to pressure changes.

Potential reference lithologies

The reference samples will be preferentially taken from mines or quarries in the Black Forest. There are a several candidates that have a lithology similar to the Soultz granites (LfU, 2000). Among these are the biotite granites Wildbad-granite, Oberkirch-granite and Friesenberg-granite and the two-mica granites Bühlertal-granite, Forbach-granite, Seebach-granite and Sprollenhaus-granite. The sites are shown in Figure 14.

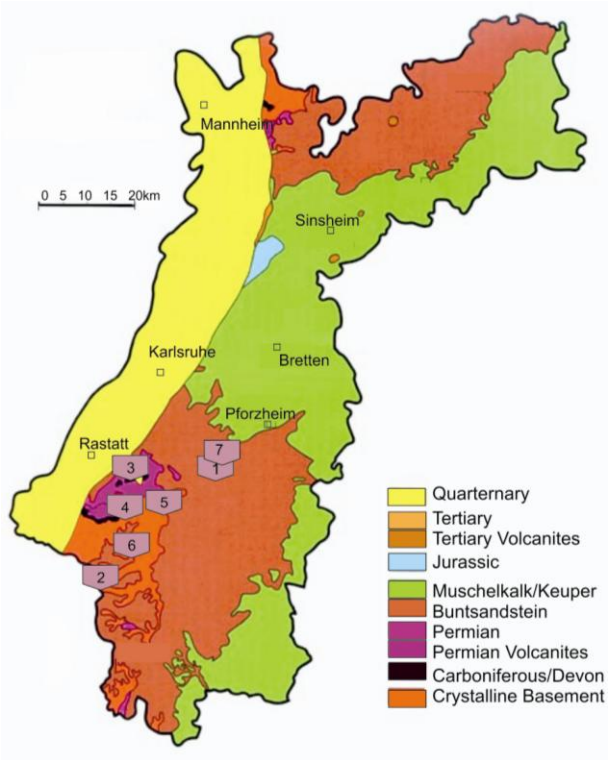

Figure 14: Geology of the district Karlsruhe. The numbers show potential reference sites in the Northern Black Forest. (1) Wildbad-granite; (2) Oberkirch-granite; (3) Friesenberg-granite; (4) Bühlertal-granite; (5) Forbach-granite; (6) Seebach-granite; (7) Sprollenhaus-granite. (modified after LfU, 2009)

CONCLUSION

With a combination of both, fracture orientation data in the prevailing stress field in Soultz-sous-Forêts, and the mechanical behavior of the fracture lithology and mineralogy, the relationship between the fracture properties and the mechanical response to pore pressure changes can be determined. This allows us to estimate the behavior of the reservoir during injection into or production from a borehole and thus might help us to better control the occurrence of microseismicity.

ACKNOWLEDGEMENTS

The authors are grateful to BRGM (France) and Dr. Chrystel Dezayes for providing the Soultz fracture datasets.

REFERENCES

Byerlee, J. (1978). "Friction of rocks." *Pure and Applied Geophysics*, **116**(4), 615-626.

Cornet, F. H., Bérard, T., and Bourouis, S. (2007) "How close to failure is a granite rock mass at a 5 km depth?" *International Journal of Rock Mechanics and Mining Sciences*, **44**(1), 47-66.

Dezayes, C., Genter, A., and Valley, B. (2010) "Structure of the low permeable naturally fractured geothermal reservoir at Soultz", Comptes Rendus Geoscience, **342**(7-8), 517-530.

Dezayes, C., Valley, B., Maqua, E., Syren, G., and Genter, A. (2000) "Natural Fracture System of the Soultz Granite based on UBI Data in the GPK3 and GPK4 Wells", *BRGM Report*, 11pp.

Fryer, R. J. (1975). "On the Subdivison of a Spherical Surface into Elements of Equal Area." *Geophys. J. R. astr. Soc.*, **42**, 883-891.

Genter, A., and Traineau, H. (1996) "Analysis of macroscopic fractures in granite in the HDR macroscopic fractures in granite in the HDR geothermal well EPS-1, Soultz-sous-Forêts, France". *Journal of Volcanology and Geothermal Research*, **72**(1-2), 121-141.

Genter, A., Castaing, C., Dezayes, C., Tenzer, H., Traineau, H., and Villemin, T. (1997) "Comparative analysis of direct (core) and indirect (borehole imaging tools) collection of fracture data in the hot dry rock Soultz reservoir (France)". *Journal of Geophysical Research, B, Solid Earth and Planets*, **102**(7), 15419-15431.

Genter, A.; Goerke, X; Graff, J.-J.; Cuenot, N.; Krall, G.; Schindler, M. and Ravier, G. (2010) "Current Status of the EGS Soultz Geothermal Project (France)". *Proceedings* World Geothermal Congress 2010, Bali, Indonesia.

Gérard, A., Genter, A., Kohl, T., Lutz, P., Rose, P., and Rummel, F. (2006) "The deep EGS (Enhanced Geothermal System) project at Soultz-sous-Forêts (Alsace, France)". *Geothermics*, **35** (5-6), 473-483.

Hooijkaas, G. R., Genter, A., and Dezayes, C. (2006) "Deep-seated geology of the granite intrusions at the Soultz EGS site based on data from 5 km-deep boreholes". *Geothermics*, **35**(5-6), 484-506.

LfU, Landesanstalt für Umweltschutz Baden-Württemberg (ed.), (2000), "Geologische Naturdenkmale im Regierungsbezirk Karlsruhe", *Bodenschutz* **5**, 2nd ed., Präzis Druck GmbH, Karlsruhe

Rummel, F., Klee, G. (1995) "State of Stress at the European HDR Candidate Sites Urach and Soultz", E. e. a. Barbier, (ed.) World Geothermal Congress. City: International Geothermal Association: Florence, Italy, pp. 2639-2642.

Terzaghi, R. D. (1965). "Sources of Error in Joint Surveys." *Geotechnique*, **15**(3), 287-.

Valley, B. (2007) "The relation between natural fracturing and stress heterogeneities in deep-seated crystalline rocks at Soultz-sous-Forêts (France)" *PhD Thesis*, ETH Zürich, Zürich.

Yow, J.L. (1987), "Blind zones in the acquisition of discontinuity orientation data". *International Journal of Rock Mechanics and Mining Sciences and Geomechanics Abstracts*, **23,** 1, pp. 19–28